Anopheles gambiae Purine Nucleoside Phosphorylase: Catalysis, Structure, and Inhibition[†,‡]

Erika A. Taylor,[§] Agnes Rinaldo-Matthis, Lei Li, Mahmoud Ghanem, Keith Z. Hazleton, María B. Cassera, Steven C. Almo, and Vern L. Schramm*

Department of Biochemistry, Albert Einstein College of Medicine at Yeshiva University, 1300 Morris Park Avenue, Bronx, New York 10461

Received May 25, 2007; Revised Manuscript Received August 15, 2007

ABSTRACT: The purine salvage pathway of *Anopheles gambiae*, a mosquito that transmits malaria, has been identified in genome searches on the basis of sequence homology with characterized enzymes. Purine nucleoside phosphorylase (PNP) is a target for the development of therapeutic agents in humans and purine auxotrophs, including malarial parasites. The PNP from *Anopheles gambiae* (AgPNP) was expressed in *Escherichia coli* and compared to the PNPs from *Homo sapiens* (HsPNP) and *Plasmodium falciparum* (PfPNP). AgPNP has k_{cat} values of 54 and 41 s^{-1} for 2′-deoxyinosine and inosine, its preferred substrates, and 1.0 s^{-1} for guanosine. However, the chemical step is fast for AgPNP at 226 s^{-1} for guanosine in pre-steady-state studies. 5′-Deaza-1′-aza-2′-deoxy-1′-(9-methylene)-Immucillin-H (DADMe-ImmH) is a transition-state mimic for a 2′-deoxyinosine ribocation with a fully dissociated N-ribosidic bond and is a slow-onset, tight-binding inhibitor with a dissociation constant of 3.5 pM. This is the tightest-binding inhibitor known for any PNP, with a remarkable K_m/K_i* of 5.4×10^7, and is consistent with enzymatic transition state predictions of enhanced transition-state analogue binding in enzymes with enhanced catalytic efficiency. Deoxyguanosine is a weaker substrate than deoxyinosine, and DADMe-Immucillin-G is less tightly bound than DADMe-ImmH, with a dissociation constant of 23 pM for AgPNP as compared to 7 pM for HsPNP. The crystal structure of AgPNP was determined in complex with DADMe-ImmH and phosphate to a resolution of 2.2 Å to reveal the differences in substrate and inhibitor specificity. The distance from the N1′ cation to the phosphate O4 anion is shorter in the AgPNP·DADMe-ImmH·PO_4 complex than in HsPNP·DADMe-ImmH·SO_4, offering one explanation for the stronger inhibitory effect of DADMe-ImmH for AgPNP.

Malaria is one of the oldest known human diseases, first described in the fifth century B.C. by Hippocrates (*1*). It was then, as it is now, a seasonal disease of the poor, being one of the principal causes of mortality in Africa, southeast Asia, and Latin America (*2*). Current World Health Organization figures estimate that malaria infection causes 300 million cases of acute illnesses and at least one million deaths annually, primarily of children under 5 years of age (*2*). In addition to the human toll, the economic costs have been estimated as 1% of world gross domestic product (GDP) per year (*3*). Attempts to break the cycle of malaria transmission include mosquito control, bed nets, antibiotics, and education, but the lack of consistent utilization of these methods has resulted in continued epidemics of malaria (*4*). Anti-malarial drugs such as chloroquine were initially successful, but drug resistance has developed and contributes to the current resurgence of the disease (*5*).

Malaria is caused by several species of *Plasmodium* that are transmitted by *Anopheles* mosquitoes when they take a human blood meal. *Plasmodium falciparum* is the most prevalent and most malignant of the malaria-causing pathogens. *P. falciparum* is a purine auxotroph, salvaging purines from its host for synthesis of RNA and DNA (*6*−*8*). Inhibition of purine salvage with transition-state analogue inhibitors is lethal for cultured malaria (*9*). Metabolic pathways for purine salvage are substantially different in *P. falciparum* and humans. The adenosine deaminase and purine nucleoside phosphorylase (PNP)[1] from the parasite accept 5′-methylthionucleosides as favorable substrates, while the respective human enzymes do not (*10*). On the basis of the differences between PfPNP and HsPNP we investigated the PNP from a mosquito vector involved in malaria transmission.

Purine metabolism in mosquitoes is now complemented by the *Anopheles gambiae* (sensu strictu strains) PEST genome sequence (*11*), thus allowing comparison of parasite,

[†] Supported by NIH Research Grant AI49512 and a fellowship from the Wenner-Gren Foundation.

* Corresponding author: telephone (718) 430-2813; fax (718) 430-8565; e-mail vern@aecom.yu.edu.

[‡] The structure of AgPNP in complex with DADMe-ImmH and PO_4^{2-} was deposited in the Protein Data Bank under ID code 2P4S.

[§] Present address: Department of Chemistry, Wesleyan University, Middletown, CT 06459.

[1] Abbreviations: DADMe, 5′-deaza-1′-aza-2′-deoxy-1′-(9-methylene); ImmH, ImmG, and ImmA, Immucillin-H, -G, and -A; PNP, purine nucleoside phosphorylase; Ag, *Anopheles gambiae*; Hs, *Homo sapiens*; Pf, *Plasmodium falciparum*; ADA, adenosine deaminase; AK, adenosine kinase; MTAP, methylthioadenosine phosphorylase; APRT, adenine phosphoribosyl transferase.

10.1021/bi7010256 CCC: $37.00
Published on Web 10/06/2007

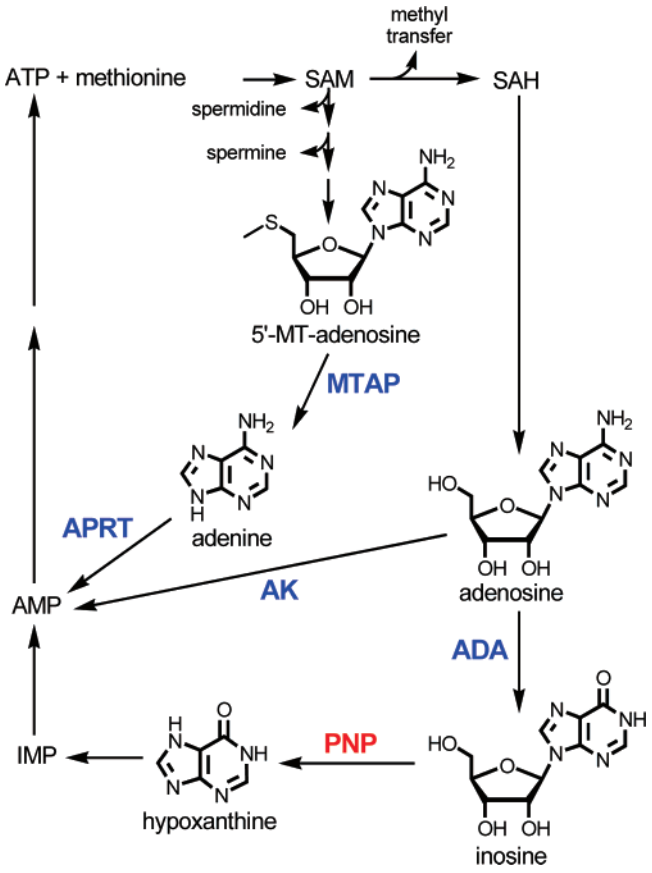

FIGURE 1: Proposed pathway for purine salvage in *A. gambiae*. On the basis of genomic sequence homology, the recycling of adenosine and MT-adenosine to AMP are likely to be similar for humans and the malarial mosquito vector.

vector, and human PNPs. Anopheline genome analysis, in comparison to the previously completed insect genomes (*12*) and the genes from previously characterized purine salvage pathways, revealed mosquito orthologues of adenosine deaminase (ADA), adenosine kinase (AK), methylthioadenosine phosphorylase (MTAP), adenine phosphoribosyltransferase (APRT), and purine nucleoside phosphorylase (PNP) (Figure 1). The anopheline PNP (AgPNP) was kinetically characterized and found to be distinct from other PNPs. AgPNP was found to be trimeric by crystallographic analysis, similar to human and bovine PNPs. Transition-state analogue inhibitors of human and malarial PNPs were also found to be powerful inhibitors of AgPNP.

MATERIALS AND METHODS

Reagents and General Methods. HsPNP and PfPNP were prepared as previously reported (*13*). Adenosine, inosine, guanosine, 2′-deoxyadenosine, 2′-deoxyinosine, 2′-deoxyguanosine, potassium phosphate, xanthine oxidase, lysozyme, and EDTA were purchased from Sigma−Aldrich Chemical Co. *Escherichia coli* competent cells (DH5α and BL21-AI), Trizol, DNase I, Superscript III reverse transcriptase, Platinum PCR super master mix High Fidelity, LR-Clonase II, L-arabinose, and pDEST-14 vectors were purchased from Invitrogen (Carlsbad, CA). Miniprep kits and Ni-NTA agarose beads were obtained from Qiagen (Valencia, CA). DNase I and protease inhibitor tablets were purchased from Roche Applied Science (Indianapolis, IN). Restriction enzymes were purchased from New England Biolabs (Ipswich). All other reagents were of the highest quality commercially available. Protein concentrations were determined by UV absorbance, by use of the extinction coefficients 28 830, 17 930, and 18 400 M^{-1} cm^{-1} at 280 nm for HsPNP, PfPNP, and AgPNP, respectively (*14*). AgPNP has no Trp residues and its concentration was also estimated by the bicinchoninic acid (BCA) assay and Bradford assays. Inhibitor concentrations were determined spectrophotometrically by use of the published millimolar extinction coefficients of 8.5 at 275 nm, 9.54 at 261 nm, and 8.92 at 269 nm at pH 7 for 9-deazaadenosine (ImmA-based inhibitors), 9-deazainosine (ImmH-based inhibitors), and 9-deazaguanosine (ImmG-based inhibitors), respectively (*15*, *16*). Substrate concentrations were determined spectrophotometrically by use of the extinction coefficients 12 200 M^{-1} cm^{-1} at 248.6 nm, 15 100 M^{-1} cm^{-1} at 260 nm, and 13 700 M^{-1} cm^{-1} at 252.5 nm for substrates containing hypoxanthine, adenine, and guanine, respectively. *Escherichia coli* cells DH5α and BL21-AI cells were grown in Luria broth (LB) with 100 μg/mL ampicillin (AMP), at 37 °C.

In Silico Purine Salvage Pathway Identification. The protein sequences *Mus musculus* ADA, *Homo sapiens* AK, *Saccharomyces cerevisiae* APRT, *H. sapiens* MTAP, and *H. sapiens* PNP (HsPNP) were used as query sequences in a tBLASTn search of the *Anopheles gambiae* genome through the NCBI web site (default settings). This database search identified hypothetical orthologues of each of these proteins with 20%, 51%, 39%, 73%, and 54% identity, respectively. Sequences were analyzed for the presence of introns, and translations of the exon regions were used for further comparisons.

RNA Isolation, cDNA Synthesis, and PCR Analysis. Genomic DNA from *A. gambiae* G3 was obtained from MR4. Total RNA was prepared directly from 7−10 frozen adults of *A. gambiae* G3 generation F5 (MRA-123B, MR4) in 2 mL of Trizol, and RNA was extracted according to the manufacturer's instructions. Subsequent cDNA synthesis was performed with 1 μg of total RNA. All RNAs were treated with DNaseI (RNase-free) before cDNA synthesis, according to the manufacturer's instructions. First strand cDNA was then synthesized by use of Superscript III reverse transcriptase and a gene-specific primer mix with 2 pmol of each antisense oligonucleotide or $(dT)_{20}$ as described by the manufacturer. Gene-specific oligonucleotide primers for *A. gambiae* PNP gene and *S7* (ribosomal protein gene), used as a control, are described in the Supporting Information. PCR reactions were performed with Platinum PCR super master mix High Fidelity as described by the manufacturer. PCR products from cDNA and gDNA of each gene were sequenced after gel purification.

Anopheles gambiae Purine Nucleoside Phosphorylase Gene Construction. A chemically synthesized gene encoding AgPNP was generated, cloned into a pDONR221 vector, and sequenced by DNA 2.0 (Menlo Park, CA). The gene was synthesized by use of optimized codons for *E. coli* protein expression and the addition of a 20-residue N-terminal thrombin-cleavable $(histidine)_6$ tag, (MetGlySerSerHisHisHisHisHisHisSerSerGlyLeuValProArgGlySerHis).

Protein Expression and Purification. The designed gene was transferred to the pDEST-14 vector with LR Clonase II. The pDEST-14-AgPNP construct was transformed into DH5α competent cells, plated onto LB-Amp, and subse-

quently grown overnight in 3 mL of LB-Amp at 37 °C. The overnight growth was pelleted and the plasmid was isolated by use of a miniprep kit. Presence of the desired gene was confirmed by separate digestion with *Avr*II and *Bam*HI. The vector was then retransformed into BL-21-AI cells. The cells were grown in LB-Amp at 37 °C to an $OD_{600} = 0.6$, induced with L-arabinose (0.2% final concentration), and then returned to 37 °C to continue growing overnight. Cells were harvested by centrifugation at 4 °C and frozen until purification.

The bacterial pellet was suspended in binding buffer (20 mM Tris-HCl, pH 7.9, 5 mM imidazole, 500 mM NaCl, and 5 mM DTT) with a spatula tip of both DNase I and lysozyme, and protease inhibitor (one tablet per 2 g of cells). The cells were ruptured by passage through a French press, and the cell debris was pelleted by centrifugation at 26000*g* for 30 min at room temperature. The remaining supernatant was incubated with 2.5 mL of Ni-NTA Agarose beads per 1 g of cell pellet for 30 min with rocking at room temperature. After incubation, the column was poured and washed with two column volumes of binding buffer. Two-column-volume stepwise fractions were taken at 100 mM imidazole and 1 M imidazole in binding buffer with AgPNP eluting in the 1 M fraction. Each fraction was eluted into a tube containing glycerol and EDTA to give final concentrations of 10% (v/v) and 1 μM, respectively. The 1 M fraction was dialyzed against 50 mM Tris-HCl pH 7.9, 10% (v/v) glycerol, 5 mM DTT, and 1 μM EDTA at room temperature. The enzyme was precipitated with 4 M $(NH_4)_2SO_4$, and stored at 4 °C. The protein was equally active with or without the $(histidine)_6$ tag, which could be removed by combining 1 unit of thrombin (GE Healthcare, Piscataway. NJ) for every 1 mg of protein in 1× PBS at 22 °C and incubating the mixture for 1 h, followed by purification over an 8 mL Source 15Q column with elution by a 0−1 M NaCl gradient in the dialysis buffer.

PNP Steady-State Assay. The phosphorolytic activity of AgPNP was determined in assay mixtures containing variable substrate concentrations (1 μM−1 mM) and 50 mM potassium phosphate, pH 7.4, at 25 °C. Inosine and adenosine activities were each measured in the xanthine oxidase-coupled spectrophotometric assays, where the conversion of hypoxanthine to uric acid was monitored at 293 nm ($\epsilon_{293} = 12.9$ mM^{-1} cm^{-1}) with 60 milliunits of xanthine oxidase or adenine conversion to 2,8-dihydroxyadenine at 301 nm ($\epsilon_{293} = 15.2$ mM^{-1} cm^{-1}) in a coupled assay with 600 milliunits of xanthine oxidase. Guanosine phosphorylase activity was measured spectrophotometrically by following the decrease in absorbance at 257 nm by converting guanosine to guanine ($\epsilon_{257} = -5.07$ mM^{-1} cm^{-1}). All reactions were initiated by the addition of enzyme, typically at 2 nM final concentration.

PNP Pre-Steady-State Assay. Enzyme was pretreated to remove hypoxanthine that copurifies with the enzyme. Two cycles of incubating for 1 min with charcoal (10% w/v) in 100 mM potassium phosphate, pH 7.4, at 25 °C were followed by centrifugation to remove tightly bound hypoxanthine. The temperature dependence of single-turnover catalysis of AgPNP with guanosine as a substrate was determined in stopped-flow fluorescence experiment. The fluorescence increase caused by enzyme-bound guanine (AgPNP·guanine·ribose-1-PO_4) was monitored at 340 nm by excitation at 295 nm, after ~6 μM of AgPNP in 100 mM KH_2PO_4, pH 7.4, was mixed with saturated guanosine (~3 mM) in the same buffer. The temperature was varied from 5 to 30 °C and at least six runs were averaged at each temperature. The pre-steady-state phosphorolytic activity of AgPNP was determined in assay mixtures containing variable substrate concentrations (0.1−0.4 mM) and 50 mM potassium phosphate, pH 7.4, at 25 °C. The enzyme was then diluted to 4 μM and a final potassium phosphate concentration of 50 mM. Bound guanine (but not free guanine or free or bound gaunosine) gives a unique fluorescence signal that can be monitored by emission at 340 nm after excitation at 290 nm; it corresponds to the formation of AgPNP·guanine·(ribose-1-PO_4) after mixing of AgPNP·PO_4 and potassium phosphate- (50 mM, pH 7.4) buffered guanosine. All values represent an average of four repeated experiments.

Slow-Onset Enzyme Inhibition Assay. Slow onset of inhibition was measured following the addition of enzyme (0.1 nM) to complete assay mixtures containing 5 mM inosine, 60 milliunits of xanthine oxidase, 50 mM potassium phosphate, pH 7.4, and inhibitor concentrations ranging from 10 μM to 2 nM, at 25 °C (*17*). The change in absorbance at 293 nm was monitored for 1−2 h to determine both the initial reaction rate and to determine whether a second reaction rate occurred as a result of slow-onset inhibition.

The K_i values were determined by fitting the initial rate and inhibitor concentrations to the following expression of competitive inhibition (*18*, *19*):

$$(V'_0/V_0) = (K_m + [S])/\{K_m + [S] + (K_m[I]/K_i)\}$$

where V'_0 is the initial rate in the presence of inhibitor and V_0 is the initial rate in the absence of inhibitor, [I] is the inhibitor concentration, and [S] is the substrate concentration. This expression is valid only under the condition where the inhibitor concentration is 10 times greater than the enzyme concentration. In conditions where inhibitor concentration does not exceed 10 times the enzyme concentration, the effective inhibitor concentration was obtained by

$$I' = I - (1 - V'_0/V_0)E_t$$

where I' is the effective inhibitor concentration, V'_0 and V_0 are the initial rates in the presence and absence of inhibitor, and E_t is the total enzyme concentration.

In cases where slow onset inhibition was observed, where the inhibitor reached a tighter binding thermodynamic equilibrium with the enzyme, the equilibrium dissociation constant (K_i*) was obtained by fitting the final rates to the following equation for competitive inhibition:

$$(V'_0/V_0) = (K_m + [S])/\{K_m + [S] + (K_m[I]/K_i^*)\}$$

with [I] concentrations being corrected as above (*16*). The K_m values for the enzymes acting on inosine are 254 μM for the mosquito enzyme, 5 μM for the malarial enzyme, and 40 μM for the human enzyme.

Crystallization of AgPNP·DADMe-ImmH Complex. In order to obtain high-quality crystals of AgPNP, the above purification procedure was followed except that the inhibitor was added to the cells prior to lysis and purification. The affinity-purified, His-tagged AgPNP·DADMe-ImmH complex was concentrated to 50 mg/mL and was stable at room temperature for weeks, whereas the protein purified in the

Table 1: Data Processing and Refinement Statistics for Ag PNP with DADMe-ImmH

wavelength, Å	1.10010
space group	$P4_12_12$
cell, Å	
$a = b$	106.7
c	240.4
resolution, Å	2.2
unique reflections	62,111
completeness,[a] %	93.9 (59.6)
multiplicity[a]	35.0 (6.6)
R_{sym},[a,b] %	10.2 (27.6)
I/σ[a]	23.3 (2.0)
no. of protein atoms	3557
no. of water	402
R-factor	17.5
R-free	21.7
avg *B*-factor, Å^2	24.7
rms bond, Å	0.02
rms angle, deg	1.72
Cruickshank's DPI value,[c] Å	0.17
Ramachandran analysis,[d] %	
allowed	99.9
disallowed	0.1

[a] Values for the highest resolution shell are given in parentheses. [b] $R_{sym} = (\Sigma_{hkl}\Sigma_i|I_i(hkl) - \langle I(hkl)\rangle|)/\Sigma_{hkl}\Sigma_i I_i(hkl)$ for n independent reflections and observations of a given reflection, $\langle I(hkl)\rangle$ is the average intensity of the ith observation. [c] The estimated error in the position of an average atom is calculated as the diffraction data precision indicator (DPI) based on R_{free} (*39*). [d] Calculated by use of MolProbity (http://molprobity.biochem.duke.edu/)

absence of inhibitor was less stable. The purified AgPNP·DADMe-ImmH complex was diluted to 30 mg/mL, and 1 mM KH_2PO_4 was added before crystallization trials. The AgPNP·DADMe-ImmH·PO_4 complex was crystallized via sitting drops that were equilibrated by vapor diffusion at 18 °C against an 80 μL reservoir containing 0.1 M sodium cacodylate trihydrate, pH 6.5, and 1.4 M sodium acetate trihydrate, where 1 μL of the protein solution was mixed with 1 μL of the reservoir solution.

Data Collection. Crystals were soaked in mother liquor supplemented with 20% glycerol and flash-cooled to −178 °C prior to data collection. Diffraction from the AgPNP·DADMe-ImmH·PO_4 crystals is consistent with the space group $P4_12_12$ ($a = b = 106.7$ Å and $c = 240.4$ Å) with three molecules in the asymmetric unit arranged in the functional trimer. The Matthews coefficient was 2.79 Å^3/Da, corresponding to a solvent content of 56%. Diffraction data were collected to a resolution of 2.2 Å at beamline X29A at the National Synchrotron Light Source, Brookhaven National Laboratory, by use of an ADSC Quantum 315 detector. Each frame was exposed for 2 s with an oscillation range of 1°. The HKL2000 suite (*20*) was used for integration and scaling of the data (see Table 1).

Structure Determination and Refinement. The structure of AgPNP in complex with DADMe-ImmH and PO_4^{2-} was solved by molecular replacement by use of a previously solved AgPNP trimer (not published), solved to 3.0 Å using a trimeric model of the human PNP (PDB code 1RR6) as a search model. Molecular replacement with PHASER (*21*, *22*), and refinement with REFMAC5 (*23*) were carried out with the CCP4i package (*24*). Arp/Warp (*25*) was used to improve the model and to add water molecules. COOT (*26*) was used for molecular modeling. Difference Fourier maps calculated with $F_o - F_c$ coefficient produced clear density at 5σ that readily allowed the inhibitor to be added to the model. Density for the 86 N-terminal residues was disordered and could not be built into the final model of the AgPNP·DADMe-ImmH·PO_4 complex. Water molecules were included in the structure following the refinement of protein and ligands. The final structure had *R*-factor and R_{free} of 17.5% and 21.7%, respectively. All structural figures were made with PYMOL (*27*).

RESULTS AND DISCUSSION

Anopheles gambiae Purine Salvage Pathway. Reports of mosquito growth on a semisynthetic medium suggested dietary requirements for AMP (or IMP), dTMP, and UMP (or CMP) or the corresponding nucleosides (*28*). Requirement for these purine metabolites suggested that purine and pyrimidine salvage pathways may play an important role in *Anopheles* nucleotide metabolism. Anopheline orthologues of previously characterized ADA, AK, MTAP, APRT, and PNP proteins were identified from the genome. The presence of genes corresponding to all five of these enzymes suggests that the purine salvage metabolic pathway resembles that found in humans (Figure 1). Alignments of these translated sequences show conservation of catalytic residues and allow assignment of consensus sequences and comparison between species (Figure 2). The AgPNP sequence is approximately 50% identical to human, bovine, and *Drosophila melanogaster* PNP sequences (54%, 55%, and 50% respectively).

General Characteristics of AgPNP. The presence of the PNP gene and its transcripts in *A. gambiae* were confirmed by PCR of *A. gambiae* genomic DNA and cDNA with a single set of primers (Supporting Information). RT-PCR analysis of the mosquito total RNA reveals that at least two splice variants of AgPNP are transcribed, a shorter variant (without the 68 N-terminal residues) and a longer variant (with the 68 N-terminal residues). The sequence corresponding to the longer variant of AgPNP protein was used to design a synthetic gene with an N-terminal histidine tag optimized for *E. coli* codon usage. This protein was highly overexpressed, yielding almost 80 mg of AgPNP/L of cultured cells after purification to >95% purity. Purification at room temperature and storage as an ammonium sulfate precipitate provided stable enzyme.

AgPNP Kinetic Parameters. The catalytic efficiencies (k_{cat}/K_m) of AgPNP were 7.0×10^4 M^{-1} s^{-1} for Ino and 2.8×10^5 M^{-1} s^{-1} for dIno (Table 2). Steady-state turnover numbers for inosine (Ino) and 2′-deoxyinosine (dIno) were 41- and 10-fold greater than for guanosine (Guo) and 2′-deoxyguanosine (dGuo), with the deoxy substrates having slightly greater k_{cat} values than their ribo analogues (Table 2). No activity was detected for adenosine or 2′-deoxyadenosine, similar to the specificity for HsPNP. AgPNP's strong preference for Ino and dIno over other purines is unique among both trimeric and hexameric PNPs (Table 3) (*17*, *29*−*32*). The AgPNP k_{cat} for inosine of 41 s^{-1} is similar to other trimeric PNPs, including those from *H. sapiens* (*33*) and *Bos taurus* (*30*), but greater than that for *P. falciparum* (*17*), which are reported to be 56, 16, and 0.34 s^{-1}, respectively (Table 4). Transition-state theory proposes that the greater the enzymatic rate enhancement for a given reaction, the greater the binding potential for a transition-state analogue (*34*). The k_{cat} value provides only an apparent

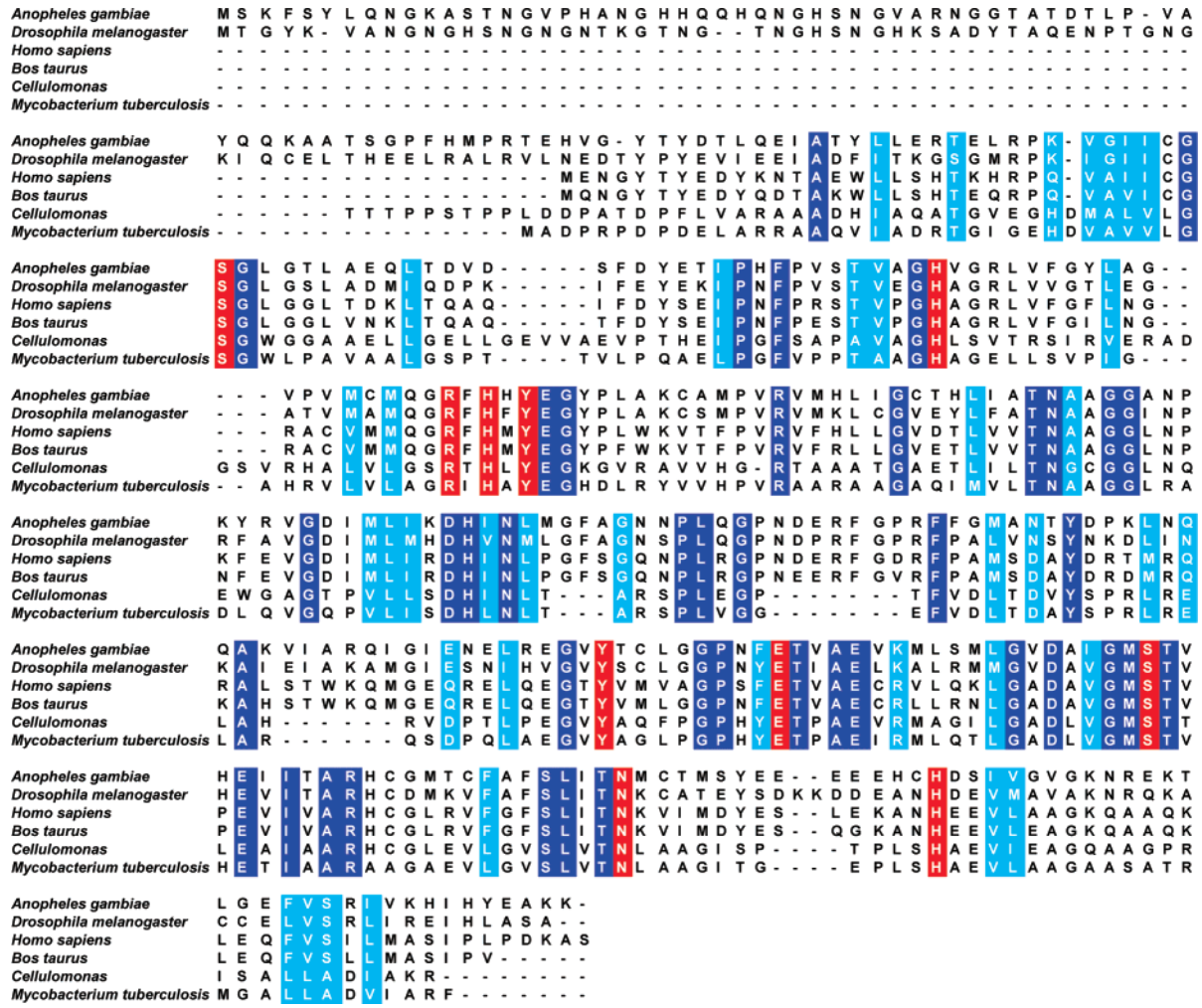

FIGURE 2: Sequence alignment of AgPNP with related enzymes (*D. melanogaster* is a putative homologue on the basis of sequence identity, whereas other enzymes are structurally characterized trimeric PNP homologues). Residues that are identical or similar are highlighted in dark or light blue, respectively. Those residues that are conserved and found in the active site are highlighted in red.

Table 2: Kinetic Constants for AgPNP with Various Substrates

substrate	k_{chem} (s^{-1})	k_{cat} (s^{-1})	K_m (μM)	k_{cat}/K_m (M^{-1} s^{-1})
inosine	nd[a]	41 ± 2	585 ± 68	7.0×10^4
guanosine	226 ± 30[b]	1.0 ± 0.2	187 ± 58	5.0×10^3
adenosine	nd	< 0.5	nd	nd
2-deoxyinosine	nd	54 ± 2	190 ± 8	2.8×10^5
2-deoxyguanosine	nd	5.4 ± 0.1	50 ± 11	1.1×10^5
2-deoxyadenosine	nd	< 0.5	n/d	n/d

[a] nd indicates that the value was not determined. [b] Reaction rate at 25 °C. Pre-steady-state turnover was also measured at other temperatures and gave a turnover of 438 ± 80 at 30 °C.

Table 3: Comparison of Substrate Utilization[a] of Various PNPs

enzyme source	multimeric state	Guo	Ino	Ado	dGuo	dIno	dAdo
A. gambiae	trimer	2	100	0	13	132	0
H. sapiens (*31*, *32*)	trimer	52	100	0	42	53	nd[b]
B. taurus (*30*)	trimer	50	100	0	38	71	nd
T. vaginalis (*29*)	hexamer	23	100	35	nd	nd	nd
E. coli (*32*)	hexamer	104	100	133	161	217	133
P. falciparum (*17*)	hexamer	41	100	0	59	188	nd

[a] Values are given as percent of V_{max} relative to inosine. [b] nd indicates that the value has not been reported in the literature.

Table 4: Kinetic Constants for Inosine with Various PNPs

enzyme source	k_{cat} (s^{-1})	K_m (μM)	k_{cat}/K_m (M^{-1} s^{-1})
A. gambiae	41	585	7.0×10^4
H. sapiens (*33*)	56	40	1.4×10^6
B. taurus (*30*)	16	36	4.4×10^5
P. falciparum (*17*)	0.34	5	6.8×10^4

value for enzymatic rate acceleration, since other PNPs have k_{cat} values limited by the rate of purine product release. The rates for chemical steps on mammalian PNPs have been reported to be 2−10-fold greater than k_{cat} (*35*, *36*). For AgPNP, the phosphorolysis of guanosine in a single-turnover on-enzyme reaction at 25 °C is 226-fold faster than k_{cat} in pre-steady-state studies (Table 2). Thus, the catalytic potential for AgPNP is greater than in mammalian enzymes, and transition-state analogue inhibitors might be expected to bind more tightly to AgPNP than to other PNPs due to the greater enzymatic rate enhancement.

Inhibition of AgPNP. The inhibition constants of AgPNP were determined for the Immucillins, known to be transition-state analogue inhibitors of HsPNP and PfPNP (Figure 3, Table 5). Unlike other PNPs, only Immucillin-H (**1**), DADMe-Immucillin-H (DADMe-ImmH; **5**), DADMe-Immucillin-G (**6**), MT-DADMe-Immucillin-H (**9**), and DADEt-Immucillin-H (**10**) exhibited slow-onset inhibition. DADMe-ImmH is the most potent inhibitor of HsPNP and was also the best inhibitor of AgPNP, having a K_i of 310 pM and a

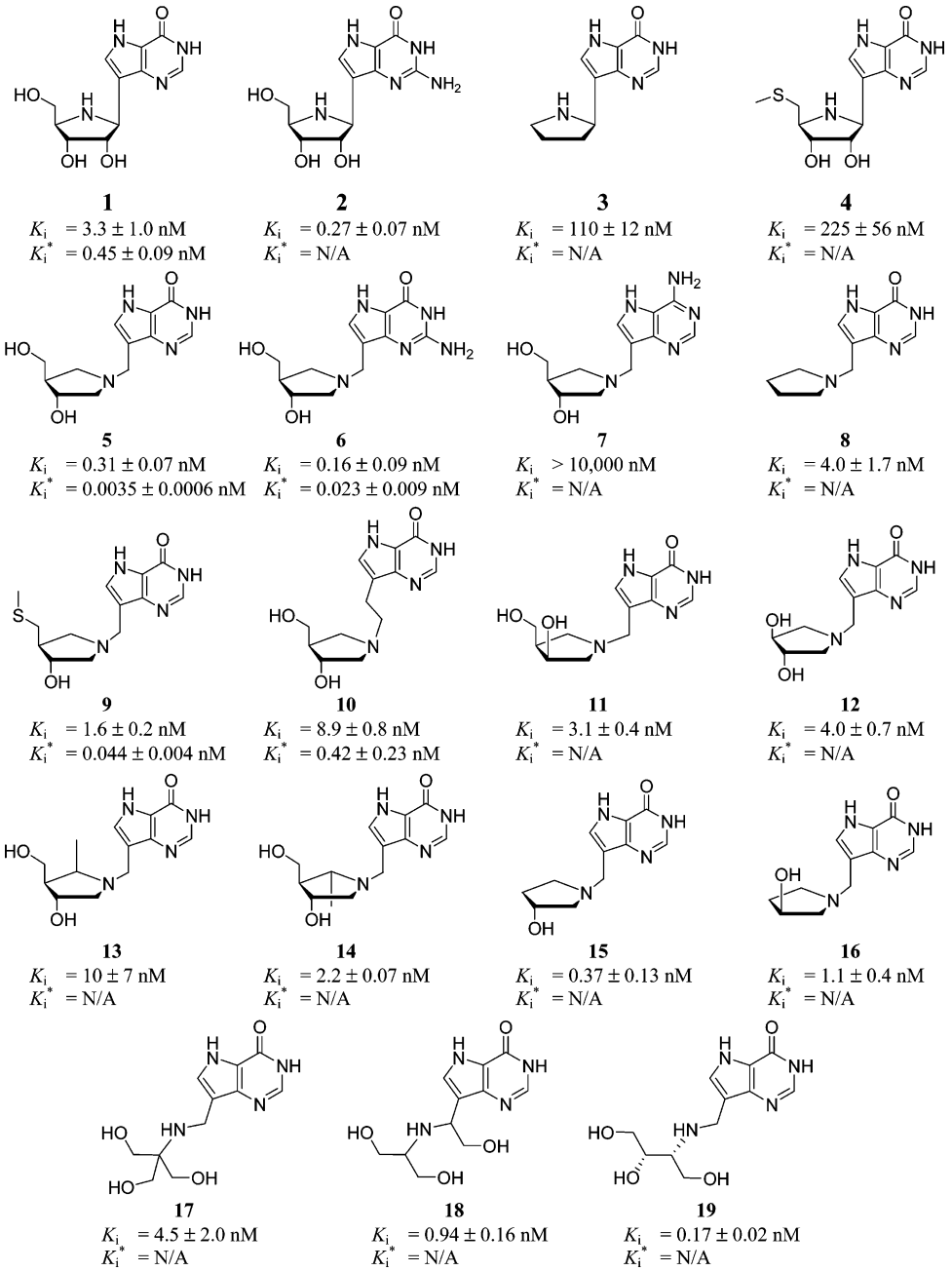

FIGURE 3: Structures and inhibition constants for inhibitors of AgPNP. All values are reported as nanomolar. K_i is initial and K_i* is final dissociation constant, as indicated under Materials and Methods. N/A indicates that no slow-onset component was observed.

K_i* of 3.5 pM. This is the tightest binding observed for any PNP inhibitor, with 2.4- and 140-fold increased affinity compared to HsPNP and PfPNP, respectively. Compounds **19**, **17**, and **18** are powerful inhibitors of HsPNP (*37*) but bind 19-, 4.5-, and 51-fold less tightly to AgPNP than to the human enzyme. Only four additional inhibitors were found to bind more tightly to HsPNP than the mosquito enzyme: Immucillin-H (**1**), Immucillin-G (**2**), DADMe-Immucillin-G (**6**), and 5″-nor-DADMe-Immucillin-H (**12**), with 7.8-, 6.4-, 3.3-, and 5.1-fold differences, respectively. MT-Immucillin-H (**4**), which has a K_i of 225 nM for AgPNP, is the only inhibitor that binds more tightly to PfPNP than AgPNP, a trend that is also true for the comparison of PfPNP and HsPNP. AgPNP bound to the remaining inhibitors with higher affinity than to HsPNP or PfPNP, which is consistent with their catalytic properties.

The tight binding of AgPNP to inhibitors without slow-onset kinetics indicates a rapid protein rearrangement to effect tight binding, whereas other PNPs require more time for this step and therefore exhibit slow-onset tight binding. Higher affinity for DADMe-ImmH (**5**) relative to Immucillin-H (**1**) suggests that AgPNP has a late, highly dissociative transition state (*38*).

Crystal Structure of AgPNP·DADMe-ImmH·PO$_4$. The structure of AgPNP·DADMe-ImmH·PO_4 is a trimer with three monomers in the asymmetric unit. The catalytic sites are formed by residues coming from a pair of monomers near the subunit interfaces. Each monomer of AgPNP has a β-sheet core flanked by seven α-helices. The monomers in the trimer of AgPNP superimpose with an rms deviation of 0.13−0.15 Å comparing Cα positions of 280 amino acid residues. The structure of AgPNP is most similar to bovine

Table 5: Inhibition Comparison of AgPNP versus HsPNP and PfPNP

inhibitor	dissociation constant[a] (nM)			relative affinity[b] (*x*-fold)	
	AgPNP	HsPNP	PfPNP	vs HsPNP	vs PfPNP
Immucillin-H (**1**)	0.47 ± 0.09	0.06 ± 0.02	0.86 ± 0.08	7.8[c]	1.8
Immucillin-G (**2**)	0.27 ± 0.07	0.042 ± 0.006	0.9 ± 0.2	6.4[c]	3.3
9-deaza-9-(pyrrolidin-2-yl)hypoxanthine (**3**)	110 ± 10	840 ± 110	273 ± 94	7.6	2.5
MT-Immucillin-H (**4**)	230 ± 60	300 ± 80	2.7 ± 0.4	1.3	85[d]
DADMe-Immucillin-H (**5**)	0.0035 ± 0.0006	0.0085 ± 0.0002	0.5 ± 0.04	2.4	140
DADMe-Immucillin-G (**6**)	0.023 ± 0.009	0.007 ± 0.001	0.89 ± 0.06	3.3[c]	39
DADMe-Immucillin-A (**7**)	>10 000	>10 000	>10 000	equal	equal
9-deaza-9-(pyrrolidin-1-ylmethyl)hypoxanthine (**8**)	4 ± 1.7	6 ± 1	6 ± 1	1.5	1.5
MT-DADMe-Immucillin-H (**9**)	0.044 ± 0.004	0.070 ± 0.009	0.89 ± 0.12	1.6	20
DADEt-Immucillin-H (**10**)	0.42 ± 0.23	0.46 ± 0.05	610 ± 150	1.1	1500
3′-epi-DADMe-Immucillin-H (**11**)	3.1 ± 0.4	4.0 ± 0.4	55 ± 9	1.3	18
5″-nor-DADMe-Immucillin-H (**12**)	4.0 ± 0.7	0.79 ± 0.34	42 ± 2	5.1[c]	11
5′-(*R*)-methyl-DADMe-Immucillin-H (**13**)	10 ± 7	34 ± 7	>10 000	3.4	>1000
5′-(*S*)-methyl-DADMe-Immucillin-H (**14**)	2.2 ± 0.7	4.0 ± 0.6	>10 000	1.8	>1000
5″-deoxy-5″-nor-DADMe-Immucillin-H (**15**)	0.37 ± 0.13	0.38 ± 0.006	1.16 ± 0.05	equal	3.1
3′-epi-5″-deoxy-5″-nor-DADMe-Immucillin-H (**16**)	1.1 ± 0.4	1.8 ± 0.2	6.4 ± 0.4	1.6	5.8
9-deaza-9-[[1,3-dihydroxy-2-(hydroxymethyl)propan-2-ylamino]methyl]hypoxanthine (**17**)	4.5 ± 2.0	0.62 ± 0.17	160 ± 80	7.3[c]	36
9-deaza-9-[1-(1,3-dihydroxypropan-2-ylamino)-2-hydroxyethyl]hypoxanthine (**18**)	0.94 ± 0.16	0.21 ± 0.08	300 ± 100	4.5[c]	320
9-deaza-9-[[(2*R*,3*S*)-1,3,4-trihydroxybutan-2-ylamino]methyl]hypoxanthine (**19**)	0.17 ± 0.02	0.0086 ± 0.0006	55 ± 12	20[c]	320

[a] Dissociation constant is defined as the tightest inhibition constant, either K_i or K_i*. [b] Affinity comparisons indicate that the inhibitor binds more tightly to the mosquito enzyme except as noted. [c] This inhibitor binds more tightly to the human enzyme. [d] This inhibitor binds more tightly to the plasmodium enzyme.

PNP (PDB code 1b80), human PNP (PDB code 1RSZ), human MTAP (PDB code 1CB0), and *E. coli* MTAN (PDB code IJYS), with rms deviations of 0.9, 0.9, 2.5, and 2.6 Å, respectively, upon comparing Cα positions of 278, 279, 229 and 226 residues. The extended N-terminal region of 86 residues could not be built into the crystal structure due to lack of electron density. The lack of density might be due to disorder or proteolytic activity in the crystallization drop during crystallization. We know from gel analysis (results not shown) that the full-length protein was used for crystallization experiments. Analysis of mRNA isolated from mosquitoes demonstrated the transcript for this form of protein (Supporting Information).

The electron density of AgPNP·DADMe-ImmH·PO_4 shows a structurally conserved water present near C2′ of bound DADMe-ImmH in human PNP, replacing the 2′-hydroxyl group found in nucleosides (PDB code 1RSZ). This water is missing in the AgPNP structure and may explain the lower K_m values for ribonucleosides as substrates. However, the tighter binding of DADMe-ImmH to AgPNP than to HsPNP is consistent with the closer contacts to DADMe-ImmH seen in the structures of AgPNP·DADMe-ImmH·PO_4 compared to HsPNP·DADMe-ImmH·SO_4. The number of close contacts, with cutoff values of 4.0 and 4.5 Å (by use of the program NCONT in the CCP4 program suite; *24*), between DADMe-ImmH and AgPNP in the complex are 25% and 15%, respectively, greater than for the same inhibitor bound to HsPNP. The ion pair between the N1′ cation of the inhibitor and the phosphate anion is also slightly shorter in the AgPNP·DADMe-ImmH·PO_4 structure, 2.7 Å, than the distance of 3.0 Å in the HsPNP·DADMe-ImmH·SO_4 structure. The presence of a sulfate instead of a phosphate ion in the HsPNP·DADMe-ImmH·SO_4 structure does not change the interactions with the protein or the inhibitor. Similar results have been seen in other experiments (unpublished) where the structure of HsPNP has been solved with both SO_4 (PDB code 1RT9) and PO_4 (PDB code 1RR6) together with Immucillin-H, and these structures show no difference in coordination at the active site.

The Thr306 residues in all subunits of AgPNP fall into the disallowed region of the Ramachandran plot, also seen in the structure of human PNP where this residue corresponds to Thr221. The side-chain hydroxyl group of Thr306 forms hydrogen bonds to the side-chain amino group of Asn200 as well as to the hydroxyl group of Ser305, which coordinates the phosphate group in the active site. The same hydrogen-bond pattern is seen in HsPNP.

Active site of AgPNP. AgPNP·DADMe-ImmH·PO_4 has the catalytic sites located at the interface between a pair of monomers. Full catalytic site occupancy is suggested by the electron density of inhibitor and phosphate in the A, B, and C subunits. While the average *B*-factors for the A, B, and C chains are 24, 27, and 22 $Å^2$, respectively, the bound ligands have *B*-factors below 20 $Å^2$, consistent with full catalytic site occupancy. The distances of hydrogen bonds described in the text are averaged values for the A, B, and C catalytic sites. Cruickshank DPI coordinate error (*39*) was 0.17 for the structure complex and rms deviation between subunits was 0.13 to 0.15 Å; therefore, a 0.3 Å cutoff was applied for significant distance differences of interaction.

The active site can be divided into purine base, sugar, and phosphate binding sites. Deazahypoxanthine is bound in a hydrophobic region formed by Phe285, Ile345, Met304, and Ile302, with Phe285 and Ile302 in hydrophobic stacking interactions. The N1 proton of the deazapurine forms a hydrogen bond to a structurally conserved water (distance 2.7 Å) that is also hydrogen-bonded to the carboxylate oxygen of Glu286 (distance of 2.6 Å). ND2 and OD1 of Asn328 make hydrogen-bond interactions to O6 and N7 of the base with distances of 3.0 and 2.7 Å, respectively. This residue is proposed to create favorable leaving-group interac-

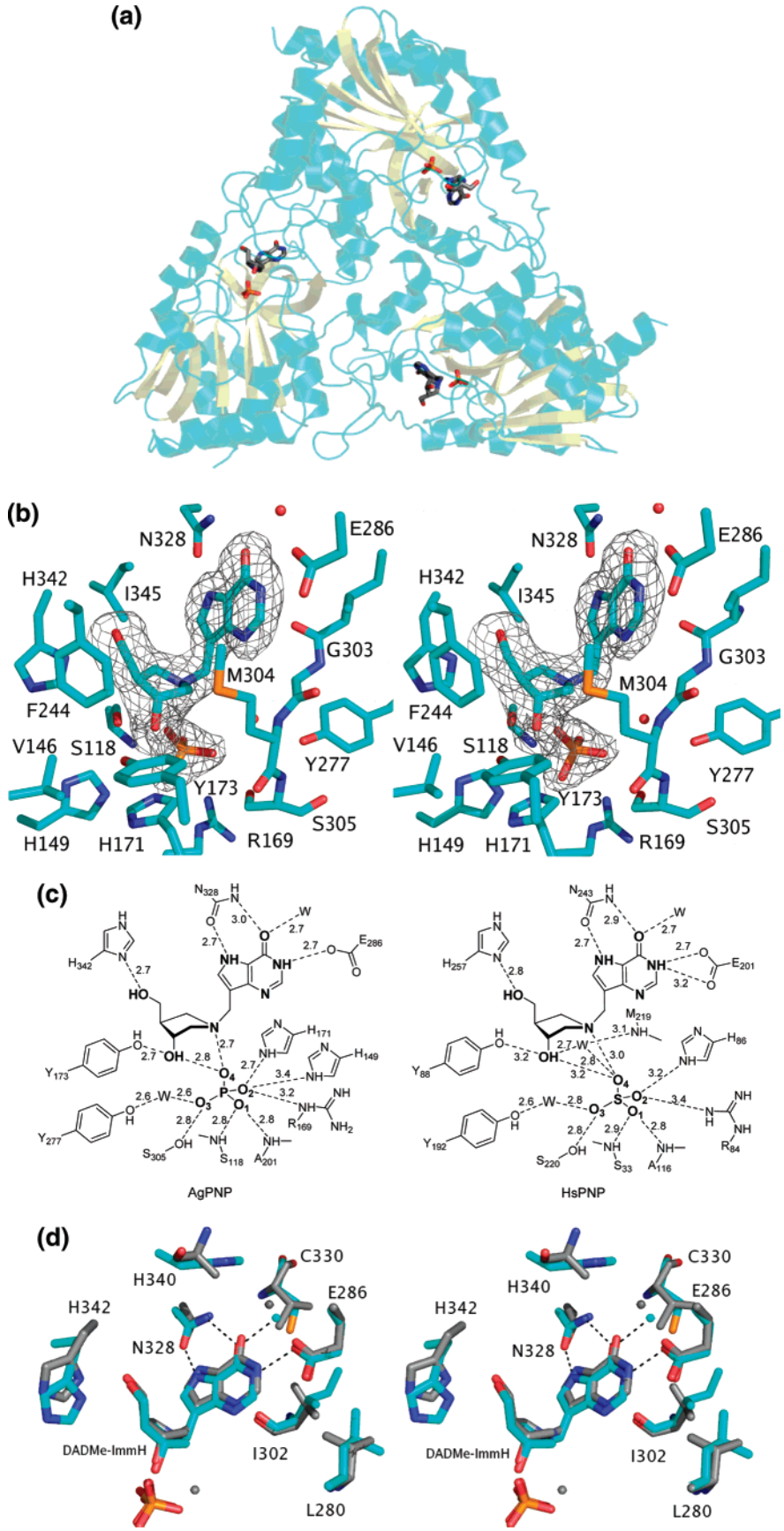

FIGURE 4: X-ray crystal structure of AgPNP with DADMe-ImmH and PO_4 bound in the active site (deposited in the Protein Data Bank under ID code 2P4S). (a) Overall structure of AgPNP in complex with DADMe-ImmH; α-helices are shown in cyan and β-strands in yellow. (b) Stereoview of the active site of AgPNP with bound DADMe-ImmH and PO_4, with electron density shown as a $F_o - F_c$ map contoured at 3σ. (c) Schematic drawing of the active-site residues in AgPNP·DADMe-ImmH·PO_4 and HsPNP·DADMe-ImmH·SO_4. (d) Stereoview superposition of HsPNP·DADMe-ImmH·SO_4 (gray) and AgPNP·DADMe-ImmH·PO_4 (cyan) to show the difference in amino acids surrounding the C2′ position of the 9-deazahypoxanthine group.

tions in mammalian PNPs, and its Asn to Asp mutation creates a nearly inactive PNP with altered base specificity (*33*). The close interaction of Asn328 and the base suggests transition-state stabilization by Asn328 through a H-bond with the N7 proton of the deazahypoxanthine leaving group. Proton stabilization by the carbonyl oxygen of Asn328 to form the transition state requires proton donation from solvent water prior to reaching the transition state (*40*).

The 3′,4′-face of the ribosyl mimic is covered by Phe244* (the asterisk indicates a contact from the adjacent subunit), which may function to occlude solvent water from the catalytic site (Figure 4b). His342 is near the 5′-hydroxyl and Tyr173 is in a H-bond interaction with the 3′-hydroxyl (2.7 Å). The 5′-OH group of the DADMe-ImmH sugar forms a hydrogen bond to ND1 of His342 (2.8 Å), and the O3′ of the sugar forms a hydrogen bond with O4 of the phosphate (2.8 Å). The N1′ of the ribose forms a 2.7 Å ion pair with O4 of the phosphate group, reducing the overall charge in the active site.

The anionic phosphate binding site is formed by Arg169, His171, and H-bond donors from the amino groups of Ser118 and Ala201. The N1′ cation of DADMe-ImmH, together with Arg169 and the dianionic phosphate, form two ion pairs with a net zero charge. The PO_4 moiety also hydrogen-bonds with the hydroxyl groups of Ser305 and Ser118. Phosphate O1 accepts hydrogen bonds from the amino groups of Ala201 (2.8 Å) and Ser118 (2.9 Å). The phosphate O2 interacts with the NE2 of His171 and the NE of Arg169, with distances of 2.7 and 3.1 Å, respectively. Phosphate O3 hydrogen-bonds to OG of Ser305 (2.8 Å) and to a structurally conserved water (2.6 Å), and phosphate O4 interacts with the 3′-OH of the DADMe-ImmH group (2.7 Å) as well as with OG of Ser118 (2.8 Å). The N1′ DADMe-ImmH cation makes an ion pair to the same PO_4 oxygen with a distance of 2.7 Å. This distance is similar to the 3.0 Å predicted from transition-state analysis of human, bovine, and *P. falciparum* PNPs. Thus, the binding of DADMe-ImmH places the phosphate oxygen nucleophile close to the actual transition state distances proposed for related PNPs (*38*, *40*, *41*). The transition-state structure of AgPNP remains to be solved, but the preferred binding of DADMe-ImmH relative to ImmH supports a fully developed carbocation at its transition state (*37*).

Comparison of AgPNP·DADMe-ImmH·PO₄ with HsPNP·DADMe-ImmH·SO₄. The catalytic mechanism proposed for AgPNP involves Asn328 activation of the hypoxanthine leaving group. In the crystal structure of AgPNP·DADMe-ImmH·PO_4, Asn328 hydrogen-bond distances are the same (within error limits) as the distances reported for HsPNP·DADMe-ImmH·SO_4 (PDB code 1RSZ). As mentioned above, the phosphate O4 anion and the N1′ cation form an ion pair 0.3 Å shorter than seen in the HsPNP (3.0 Å). Ion-pair energy in a low dielectric is highly dependent on distance, and this difference is consistent with the differences in inhibitor affinity. Although there are many similarities between AgPNP·DADMe-ImmH·PO_4 and HsPNP·DADMe-ImmH·SO_4, the loss of a structural water close to C2′ of DADMe-ImmH is a significant difference. This water occupies a space similar to the 2′-OH group in the ribo sugars and may explain the lower affinity of AgPNP for nucleosides than in HsPNP. The inability of AgPNP to stabilize a water molecule at this site suggests an inability to stabilize the 2′-OH in the nucleoside substrates. The absence of this water in AgPNP might also allow for closer bonding interactions between N1′ and 3′-OH of the inhibitor to both the protein and the phosphate. His149 in AgPNP (His64 in the HsPNP) is positioned on a loop that interacts with phosphate (3.4 Å), similar to that in the BtPNP·ImmH·PO_4 (*40*) and HsPNP·DATMe-ImmH·SO_4 complexes but distinct from the HsPNP·DADMe-ImmH·SO_4 complex (11 Å distant).

Studies of substrate and inhibitor binding indicate that AgPNP has a surprisingly low affinity for substrates or inhibitors with an amino group at the C2 position. Comparison of HsPNP and AgPNP near the substrate C2 position identifies two residues that differ. The more bulky Ile302 and Leu280 residues in AgPNP are substituted by valines in human PNP and may explain the observed difference in substrate specificity.

CONCLUSIONS

AgPNP is unique in its substrate specificity. Its rapid pre-steady-state turnover number for guanosine supports high catalytic potential. The transition-state analogue DADMe-ImmH resembles a fully dissociated 2′-deoxyinosine ribooxacarbenium transition state and is a powerful, slow-onset, tight-binding inhibitor for AgPNP with a K_i* value of 3.5 pM and a K_m/K_i* value of 5.4×10^7. 2′-Deoxyinosine is the most favorable substrate for AgPNP, and the inhibition pattern suggests that AgPNP forms a fully dissociated transition state in the phosphorolysis of 2′-deoxyinosine. AgPNP is highly selective for transition-state analogues, with DADMe-ImmH binding being preferred relative to other transition-state analogues. The structure of AgPNP is similar to other trimeric PNPs, although an 86 residue N-terminal region of AgPNP is disordered. The mRNA encoding this protein and an N-terminal splice variant are both present in mosquito extracts. Comparison with HsPNP, which binds DADMe-ImmH with a dissociation constant of 9 pM, allows observation of some differences in the structures, which might correspond to differences in the binding affinity of transition-state analogues. The structure of the AgPNP complex reveals that a conserved water molecule is missing in AgPNP, which may influence the substrate specificity and the tighter binding of DADMe-ImmH. The N1′ cation to phosphate-O4 anion distance is shorter (2.7 Å) in the AgPNP·DADMe-ImmH·PO_4 compared to HsPNP·DADMe-ImmH·SO_4, suggesting that the AgPNP transition state may include weak nucleophile participation by the phosphate. AgPNP has low k_{cat} values for guanosine substrates and relatively weak binding to transition-state analogues of guanosine. For guanosine, burst kinetics indicate rate-limiting product release in the catalytic cycle. Larger residues (Ile and Leu) in proximity to the C2 position of DADMe-ImmH make the region sterically hindered for C2−NH_2 interactions.

ACKNOWLEDGMENT

We thank the staff at NSLS Brookhaven National Lab for technical assistance at X29A. Also, we thank Dr. Emilio F. Merino at New York University for his help with sequence analysis. We thank MR4 for providing us with *Anopheles gambiae* mosquitoes and genomic DNA contributed by Mark Q. Benedict and William E. Collins.

SUPPORTING INFORMATION AVAILABLE

Gene-specific oligonucleotide primers, PCR of genomic DNA and cDNA, and analysis of mRNA isolated from mosquitoes. This material is available free of charge via the Internet at http://pubs.acs.org.

REFERENCES

1. Gilles, H. M. (2002) in *Essential Malariology* (Warrell, D. A., and Gilles, H. M., Eds.) pp 1−7, Arnold, New York.
2. World Health Organization (2007) *Malaria*, Fact Sheet No. 94, Geneva, Switzerland.
3. Sachs, J. D., and Malaney, P. (2002) The economic and social burden of malaria, *Nature 415*, 680−685.
4. Sachs, J. D. (2002) A new global effort to control malaria, *Science 298*, 122−124.
5. Wellems, T. E. (2002) *Plasmodium* chloroquine resistance and the search for a replacement antimalarial drug, *Science 298*, 124−125.
6. Sherman, I. W. (1998) in *Parasite Biology, pathogenesis and protection* (Sherman, I. W., Ed.) pp 89−117, ASM Press, Washington, DC.
7. Stoeckler, J. D. (1984) Purine nucleoside phosphorylase: A target for chemotherapy, in *Development in Cancer Chemotherapy* (Glazer, R. I., Ed.) pp 35−60, CRC Press, Inc., Boca Raton, FL.
8. de Koning, H. P., Bridges, D. J., and Burchmore, R. J. S. (2005) Purine and pyrimidine transport in pathogenic protozoa: From biology to therapy, *FEMS Microbiol. Rev. 29*, 987−1020.
9. Kicska, G. A., Tyler, P. C., Evans, G. B., Furneaux, R. H., Schramm, V. L., and Kim, K. (2002) Purine-less death in *Plasmodium falciparum* induced by Immucillin-H, a transition state analogue of purine nucleoside phosphorylase, *J. Biol. Chem. 277*, 3226−3231.
10. Ting, L. M., Shi, W., Lewandowicz, A., Singh, V., Mwakingwe, A., Birck, M. R., Taylor, Ringia, E. A., Bench, G., Madrid, D. C., Tyler, P. C., Evans, G. B., Furneaux, R. H., Schramm, V. L., and Kim, K. (2005) Targeting a novel *Plasmodium falciparum* purine recycling pathway with specific immucillins, *J. Biol. Chem. 280*, 9547−9554.
11. Holt, R. A., Subramanian, G. M., Halpern, A., Sutton, G. G., Charlab, R., Nusskern, D. R., Wincker, P., Clark, A. G., Ribeiro, J. M. C., Wides, R., Salzberg, S. L., Loftus, B., Yandell, M., Majoros, W. H., Rusch, D. B., Lai, Z., Kraft, C. L., Abril, J. F., Anthouard, V., Arensburger, P., Atkinson, P. W., Baden, H., de Berardinis, V., Baldwin, D., Benes, V., Biedler, J., Blass, C., Bolanos, R., Boscus, D., Barnstead, M., Cai, S., Center, A., Chatuverdi, K., Christophides, G. K., Chrystal, M. A., Clamp, M., Cravchik, A., Curwen, V., Dana, A., Delcher, A., Dew, I., Evans, C. A., Flanigan, M., Grundschober-Freimoser, A., Friedli, L., Gu, Z., Guan, P., Guigo, R., Hillenmeyer, M. E., Hladun, S. L., Hogan, J. R., Hong, Y. S., Hoover, J., Jaillon, O., Ke, Z., Kodira, C., Kokoza, E., Koutsos, A., Letunic, I., Levitsky, A., Liang, Y., Lin, J.-J., Lobo, N. F., Lopez, J. R., Malek, J. A., McIntosh, T. C., Meister, S., Miller, J., Mobarry, C., Mongin, E., Murphy, S. D., O'Brochta, D. A., Pfannkoch, C., Qi, R., Regier, M. A., Remington, K., Shao, H., Sharakhova, M. V., Sitter, C. D., Shetty, J., Smith, T. J., Strong, R., Sun, J., Thomasova, D., Ton, L. Q., Topalis, P., Tu, Z., Unger, M. F., Walenz, B., Wang, A., Wang, J., Wang, M., Wang, X., Woodford, K. J., Wortman, J. R., Wu, M., Yao, A., Zdobnov, E. M., Zhang, H., Zhao, Q., Zhao, S., Zhu, S. C., Zhimulev, I., Coluzzi, M., della Torre, A., Roth, C. W., Louis, C., Kalush, F., Mural, R. J., Myers, E. W., Adams, M. D., Smith, H. O., Broder, S., Gardner, M. J., Fraser, C. M., Birney, E., Bork, P., Brey, P. T., Venter, J. C., Weissenbach, J., Kafatos, F. C., Collins, F. H., and Hoffman, S. L. (2002) The genome sequence of the malaria mosquito *Anopheles gambiae*, *Science 298*, 129−149.
12. Kaufman, T. C., Severson, D. W., and Robinson, G. E. (2002) The *Anopheles* genome and comparative insect genomics, *Science 298*, 97−98.
13. Lewandowicz, A., Taylor Ringia, E. A., Ting, L. M., Kim, K., Tyler, P. C., Evans, G. B., Zubkova, O. V., Mee, S., Painter, G. F., Lenz, D. H., Furneaux, R. H., and Schramm, V. L. (2005) Energetic mapping of transition state analogue interactions with human and *Plasmodium falciparum* purine nucleoside phosphorylases, *J. Biol. Chem. 280*, 30320−30328.
14. Extinction coefficients were determined by use of the Protparam tool (www.expasy.org/tools/protparam/html).
15. Miles, R. W., Tyler, P. C., Furneaux, R. H., Bagdassarian, C. K., and Schramm, V. L. (1998) One-third-the-sites transition-state inhibitors for purine nucleoside phosphorylase, *Biochemistry 37*, 8615−8621.
16. Singh, V., Evans, G. B., Lenz, D. H., Mason, J. M., Clinch, K., Mee, S., Painter, G. F., Tyler, P. C., Furneaux, R. H., Lee, J. E., Howell, P. L., and Schramm, V. L. (2005) Femtomolar transition state analogue inhibitors of 5′-methylthioadenosine/S-adenosylhomocysteine nucleosidase from *Escherichia coli*, *J. Biol. Chem. 280*, 18265−18273.
17. Kicska, G. A., Tyler, P. C., Evans, G. B., Furneaux, R. H., Kim, K., and Schramm, V. L. (2002) Transition state analogue inhibitors of purine nucleoside phosphorylase from *Plasmodium falciparum*, *J. Biol. Chem. 277*, 3219−3225.
18. Merkler, D. J., Brenowitz, M., and Schramm, V. L. (1990) The rate constant describing slow-onset inhibition of yeast AMP deaminase by coformycin analogs is independent of inhibitor structure, *Biochemistry 29*, 8358−8364.
19. Singh, V., Shi, W., Evans, G. B., Tyler, P. C., Furneaux, R. H., Almo, S. C., and Schramm, V. L. (2004) Picomolar transition state analogue inhibitors of human 5′-methylthioadenosine phosphorylase and X-ray structure with MT-Immucillin-A, *Biochemistry 43*, 9−18.
20. Otwinowski, Z., and Minor, W. (1997) Processing of X-ray diffraction data collected in oscillation mode, *Methods Enzymol. 276*, 307−326.
21. Read, R. J. (2001) Pushing the boundaries of molecular replacement with maximum likelihood, *Acta Crystallogr. D57*, 1373−1382.
22. Storoni, L. C., McCoy, A. J., and Read, R. J. (2004) Likelihood enhanced fast rotation functions, *Acta Crystallogr. D59*, 1145−1153.
23. Murshudov, G. N., Vagin, A. A., and Dodson, E. J. (1997) Refinement of macromolecular structures by the maximum-likelihood method, *Acta Crystallogr. D53*, 240−255.
24. Potterton, E., Briggs, P., Turkenburg, M., and Dodson, E. J. (2003) A graphical user interface to the CCP4 program suite, *Acta Crystallogr. D59*, 1131−1137.
25. Lamzin, V. S., and Wilson, K. S. (1993) Automated refinement of protein models, *Acta Crystallogr. D49*, 129−147.
26. Emsley, P., and Cowtan, K. (2004) Model-building tools for molecular graphics, *Acta Cryst. D60*, 2126−2132.
27. DeLano, W. L. (2002) The PyMOL molecular graphics system, San Carlos, CA.
28. Clements, A. N. (1992) *The biology of mosquitoes*, Vol. 1, Chapman and Hall, New York.
29. Rinaldo-Matthis, A., Wing, C., Ghanem, M., Deng, H., Wu, P., Gupta, A., Tyler, P. C., Evans, G. B., Furneaux, R. H., Almo, S. C., Wang, C. C., and Schramm, V. L. (2007) Inhibition and structure of *Trichomonas vaginalis* purine nucleoside phosphorylase with picomolar transition state analogues, *Biochemistry 46*, 659−668.
30. Barsacchi, D., Cappiello, M., Tozzi, M. G., Del, Corso, A., Peccatori, M., Camici, M., Ipata, P. L., and Mura, U. (1992) Purine nucleoside phosphorylase from bovine lens: purification and properties, *Biochim. Biophys. Acta 1160*, 163−170.
31. Stoeckler, J. D., Cambor, C., and Parks, R. E. (1980) Human erythrocytic purine nucleoside phosphorylase: Reaction with sugar-modified nucleoside substrates, *Biochemistry 19*, 102−107.
32. Bzowska, A., Kulikowskaa, E., and Shugar, D. (2000) Purine nucleoside phosphorylases: properties, functions, and clinical aspects, *Pharmacol. Ther. 88*, 349−425.
33. Erion, M. D., Takabayashi, K., Smith, H. B., Kessi, J., Wagner, S., Hoenger, S., Shames, S. L., and Ealick, S. E. (1997) Purine nucleoside phosphorylase. 1. Structure−function studies, *Biochemistry 36*, 11725−11734.
34. Schramm, V. L. (1998) Enzymatic transition states and transition state analog design, *Annu. Rev. Biochem. 67*, 693−720.
35. Bzowska, A. (2002) Calf spleen purine nucleoside phosphorylase: complex kinetic mechanism, hydrolysis of 7-methylguanosine, and oligomeric state in solution, *Biochim. Biophys. Acta 1596*, 293−317.
36. Kline, P. C., and Schramm, V. L. (1993) Purine nucleoside phosphorylase. Catalytic mechanism and transition-state analysis of the arsenolysis reaction, *Biochemistry 32*, 13212−13219.
37. Taylor, E. A., Clinch, K., Kelly, P. M., Li, L., Evans, G. B., Tyler, P. C., and Schramm, V. L. (2007) Acyclic ribooxacarbenium ion

mimics as transition state analogues of human and malarial purine nucleoside phosphorylases, *J. Am. Chem. Soc. 129*, 2985−2987.
38. Taylor Ringia, E. A., Tyler, P. C., Evans, G. B., Furneaux, R. H., Murkin, A. S., and Schramm, V. L. (2006) Transition state analogue discrimination by related purine nucleoside phosphorylases, *J. Am. Chem. Soc. 128*, 7126−7127.
39. Cruickshank, D. W. (1999) Remarks about protein structure precision, *Acta Crystallogr. D55*, 583−601.
40. Fedorov, A., Shi, W., Kicska, G., Fedorov, E., Tyler, P. C., Furneaux, R. H., Hanson, J. C., Gainsford, G. J., Larese, J. Z., Schramm, V. L., and Almo, S. C. (2001) Transition State Structure of Purine Nucleoside Phosphorylase and Principles of Atomic Motion in Enzymatic Catalysis, *Biochemistry 40*, 853−860.
41. Schramm, V. L. (2003) Enzymatic transition state poise and transition state analogues, *Acc. Chem. Res. 36*, 588−596.

BI7010256